

Classification of Paddy Rice Using a Stacked Generalization Approach and the Spectral Mixture Method Based on MODIS Time Series

Meng Zhang¹, Huaiqing Zhang, Xinyu Li, Yang Liu, Yaotong Cai, and Hui Lin

Abstract—Paddy rice is a major staple food, accounting for about 20% world's food supply. And the rice paddy, an important artificial wetland type, plays an important role in the regional ecological environment. This study proposes a stacked generalization and spectral mixture approach to map paddy rice using coarse spatial resolution images [Moderate Resolution Imaging Spectralradiometer, (MODIS)]. By this method, the time series MODIS enhanced vegetation index images, phenological variables, land surface water index, elevation, and slope images are all employed to produce the optimal feature combination, which is then used to map paddy rice by the stacking algorithm. The validation experiment using the data of the Dongting Lake area showed that the proposed method can improve the overall accuracy of single classifiers, including the support vector machine, random forest, k-nearestneighbor (kNN), extreme gradient boosting (XGB), and decision tree. Stacking (XGB) achieves the highest overall accuracy (90.3%) and Kappa coefficient (0.86), which are 2.8% and 0.03 higher than that of using the single kNN classifier. Furthermore, its user accuracies for distinguishing double-cropping rice and single-season rice are 92.5% and 90.0%, respectively. In terms of the paddy rice classification accuracy, the stacking model is also superior to single classifiers. Moreover, the MODIS-derived rice map obtained by the stacked generalization approach and the spectral mixture method area has a large determination coefficient ($R^2 = 0.9975$) with the government statistic data. The results demonstrate the potential of the proposed method in using coarse spatial resolution images for large-scale paddy rice mapping.

Index Terms—Moderate Resolution Imaging Spectralradiometer (MODIS) time series, paddy rice, phenological variables, spectral mixture, stack generalization.

I. INTRODUCTION

PADDY rice feeds 1/5 of the world's people. The demand for paddy rice is increasing due to the fast-growing global population and cause cultivate land and water shortage and biodiversity damage [1]–[5]. As an important cultivated wetland, rice paddy consumes a large amount of fresh water and

Manuscript received December 10, 2019; revised April 17, 2020; accepted May 4, 2020. Date of publication May 14, 2020; date of current version May 29, 2020. This work was supported in part by the National Natural Science Foundation of China under Grant 41901385, and in part by the China Postdoctoral Science Foundation under Grant 2019M652815. (Corresponding author: Hui Lin.)

Meng Zhang, Xinyu Li, Yaotong Cai, and Hui Lin are with the Central South University of Forestry and Technology, Changsha 410004, China (e-mail: mengzhang@csuft.edu.cn; lxy365@163.com; yaotongcai@csuft.edu.cn; linhui@csuft.edu.cn).

Huaiqing Zhang and Yang Liu are with the Research Institute of Forest Resources Information Techniques, Chinese Academy of Forestry, Beijing 100091, China (e-mail: zhang@ifrit.ac.cn; liuyangifrit@gmail.com).

Digital Object Identifier 10.1109/JSTARS.2020.2994335

emits massive methane (CH_4) into the atmosphere, so it has a significant influence on atmospheric chemistry and climate change [6]–[9]. Therefore, large-scale paddy rice field monitoring is of great importance for food security, water resources exploration, and environment sustainable development. Conventional paddy rice mapping is based on land inventory at the subcounty or subprovince level [10]. However, the census data cannot demonstrate accurate spatial distribution and temporal dynamics. Satellite images, such as Moderate Resolution Imaging Spectralradiometer (MODIS)-based MCD12Q1 [11], MERIS-based GlobCover [12], MERIS and SPOT-VGT based CCI-LC [13], and Landsat-based FROM-GLC [14] have been used to generate paddy rice maps. Although these data are easily available, they are not timely updated, so they cannot get wide applications in the regions with rapid economic development and climate changes. Therefore, annually updated datasets of rice production area and high spatial resolution distribution maps at different scales are imperative.

Global imaging sensors can provide data for mapping paddy rice areas on a global, continental, or regional scale [15]–[25]. The advanced very high-resolution radiometer and MODIS are two widely used sensors in this field. The freely available MODIS data has a wide coverage and high spectral-temporal resolutions, so they have been increasingly employed for rice mapping and monitoring [26], [27]. Furthermore, time-series MODIS images show superiority in land-use type classification and crop monitoring, as they can extract vegetation information at different growing stages [28]–[34]. Among the time-series MODIS data, spectral [35]–[37], land surface water index (LSWI) [17], [38], and vegetation index [e.g., normalized different vegetation index (NDVI) and enhanced vegetation index (EVI)] [39]–[41] have been widely used in monitoring and mapping rice cultivated areas, because of their high temporal resolutions. EVI is more consistent with the *in situ* phenology data than NDVI [42]. The phenological parameters derived from time series vegetation indexes also can help improve the accuracy of paddy rice mapping [43], [44]. So this study uses the EVI time series and the phenological parameters derived from it to map paddy rice.

Most conventional paddy rice mapping studies based on MODIS data use the pixel-based image analysis algorithm and has made a great contribution to paddy rice monitoring. Xiao *et al.* [17], [18] used several vegetation indices (LSWI, EVI, and NDVI) derived from MODIS images (500 m) to map paddy

rice fields in southern China and southeastern Asia by a threshold method. They achieved correlations of $R^2 = 0.88$ for flat regions and $R^2 = 0.80$ for hilly regions between the MODIS-derived rice and the National Land Cover Project dataset in southern China and obtained correlation of $R^2 = 0.97$ between the MODIS-derived rice and national agriculture statistical data in southeastern Asia. Son *et al.* [4] and Sakamoto *et al.* [27], [45] employed the EVI time series and growth calendar of paddy rice (phenology features) to identify rice area from 2000–2005 to 2000–2012, respectively, in Mekong Delta of Vietnam, and achieved an average overall accuracy of about 80% and Kappa coefficient of 0.7. Teluguntla *et al.* [38] got the flooded paddy rice maps in the Krishna River Basin, India, using multitemporal MODIS images and the DT method. The accuracy of the paddy rice maps is approximately 78%. Thenkabail [36] evaluated the capability of time-series MODIS image and fuzzy classification (ISODATA and decision tree) for paddy rice mapping in south Asia and achieved a nearly 70% overall accuracy and correlation $R^2 = 0.97$ between the MODIS derived rice and the subnational statistics data. Although there are lots of classifier algorithms for paddy rice extraction based on the MODIS dataset, a method that can improve the classification accuracy for different or specific scenarios based on these classifier algorithms is needed.

Classification is a basic task of data mining and machine learning. How to improve the performance of classifiers is the focus of relating researches [46]. Traditional classifiers, including support vector machine (SVM) and DT, are often adopted by learning classifier systems to train a set of samples to form a model. Then the trained model is used to predict new test samples [47]. However, with the increasing amount and diversification of data, these traditional classification algorithms cannot process existing data and solve practical problems well. Ensemble algorithms of single classifiers show superiority in classification [48]. Those methods combine some weak prediction models to form a good prediction model [48]. Now, some ensemble methods, including boosting, bagging, and stacking, have been employed in classification researches [49]. The performance of the bagging method depends on the stability of its base classifiers. It works well for unstable classification algorithms (DT, neural network, etc.), but it is not ideal for the integration of stable classifiers [50]. The training set of the base classifier of the boosting method is determined by the classification performance of the previous base classifier and the samples that are faulty for the previous base classifier that appear in the training set of next base classifier with a higher probability. Although the generalization performance of the combined classification algorithm is improved, there may be too much bias in some conditions, which may decrease the classification accuracy [51]. Stacking achieves the optimal generalization on the basis of different algorithms and secondary learning. The stacking method, with a strong ability of nonlinear representation and generalization error reduction, is designed to solve both bias (boosting) and variance (bagging) [52].

This article develops a comprehensive framework for mapping paddy rice using multitemporal MODIS data. An ensemble of classification algorithm (stacking method) is used together to achieve paddy rice maps of high accuracy and sensitivity.

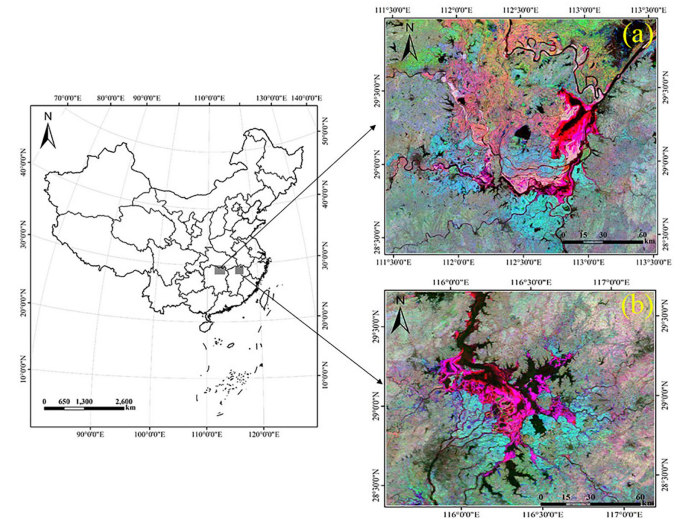


Fig. 1. Study sites (false-color composite, NIR: MODIS EVI on DOY241, Red: MODIS EVI on DOY145, and Green: MODIS EVI on DOY 65). (a) Dongting Lake area. (b) Poyang Lake area.

The validation experiments have been done in two commodity grain bases of China. In addition, the spectral mixture method is applied to obtain the rice planting area in the study area. The government statistics as well as the National Land Cover Dataset are used to validate the proposed approach. The proposed method can be used to solve complex land cover classification problems.

II. STUDY AREA AND DATA

A. Study Area

The Dongting Lake area is located in the middle reach of the Yangtze River, southern China [see Fig. 1(a)]. The area is featured by a subtropical monsoon humid climate. It has four distinct seasons. The average annual temperature is 15–18 °C and the annual precipitation is about 420 mm. This region has a complicated water system with dense river networks. It is one of the largest commodity grain base in China, growing double- and single-cropping rice. The double-cropping rice has the early rice growing between April and July and the late rice growing between July and October. And the single-season rice grows during June–September. Dongting Lake is the second-largest freshwater lake in China, and it is also an important natural wetland in China [53]. The vegetation grows in wetland, such as sedge and reed, is easily confused with paddy rice. From 1950 to 1980, a large area of wetlands was reclaimed for rice cultivation to solve the food shortage. In recent years, the Chinese government promulgated a series of wetland protection policies, including returning farmland to lakes. So a lot of farmlands have been transformed into wetlands. Therefore, accurate estimation and monitoring of rice planting area in the Dongting Lake area is not only important to national food security but also provides technical support for the regional ecological environmental protection. The Poyang Lake area [see Fig. 1(b)] is selected to validate the method proposed in this article. Poyang Lake is the largest freshwater lake in China, which is also located in

the middle reach of the Yangtze River and has similar climatic conditions with Dongting Lake. Additionally, the Poyang Lake area is also an important natural wetland reserve and commodity grain base in China. The phenological period of rice growth there is similar to that of the Dongting Lake area. In this article, the main body of the lake and the counties or districts with large rice distribution areas around the lake in the Dongting Lake area and Poyang lake area are studied.

B. Data and Processing

In this study, EVI, LSWI, phenological parameters, and DEM were employed to map the paddy rice in the Dongting Lake area and Poyang Lake area. Google earth images, Sentinel-2 MSI images, and the 1:10000 land use/land cover (LULC) map were used to assist in identifying the cover types and collecting samples for training and testing models. In the sample selection, Google Earth and land use data are the main data, while sentinel-2 is only an assistant. Field data, Statistical Yearbook, and the National Land Cover Dataset (NLCD) 2010 were employed to validate the proposed method.

We used the 16-day composited vegetation index products (MOD13Q1) of the MODIS data, which has a spatial resolution of 250 m in the sinusoidal projection. The data were obtained between January 1st and December 31st in 2018 by the USGS. MOD13Q1 has NDVI, EVI, and four spectral bands, which are blue (459–479 nm), red (620 -670 nm), near infrared (NIR) (841–876), and shortwave NIR (SWIR-2) (2105–2155 nm). LSWI is calculated by $LSWI = (NIR-SWIR-2)/(NIR + SWIR-2)$ [54]. Band SWIR with a resolution of 500 m was resampled to get a resolution of 250 m, which is the same as that of other bands and the vegetation index. After removing the invalid values from MOD13Q1 by pixel reliability images, we transformed all MODIS datasets to UTM (WGS84) projection, zone 49 (North) using ENVI5.1. In this study, EVI and LSWI were used to map paddy rice.

The clear (0% cloud cover) Sentinel-2 images over the study area (path/row: N0205_R075_T49RFM) were acquired in 2018 and downloaded from the European Space Agency website. The Sentinel-2 image has 13 bands, including visible, NIR, and short-wave bands, among which the five NIR bands (four red edge bands and one NIR band) can be used for vegetation monitoring and analysis. The topography effects and atmospheric delay in the Level-1C data were removed or reduced by the SRTM DEM and the Sen2Cor algorithm, respectively [55]. Moreover, 23 ground control points were selected to register the Sentinel-2A images. All images were georeferenced to the UTM projection, zone 49N. The processed Sentinel-2 MSI images were used to assist in the selection of training samples.

We did a field survey between April 1st and July 31st, 2018, when paddy rice fields were in flooding or transplanting. The field site of each land cover type has a width and length larger than 250 m. The field sites include double-season rice, single-season rice, sedge, reed, and others. “Others” includes, but is not limited to, forest, rain-fed cropland, water, and built up. The number of the field sites for double-cropping rice, single-season rice, sedge, reed, and others are 32, 30, 25, 22, and 36 [see

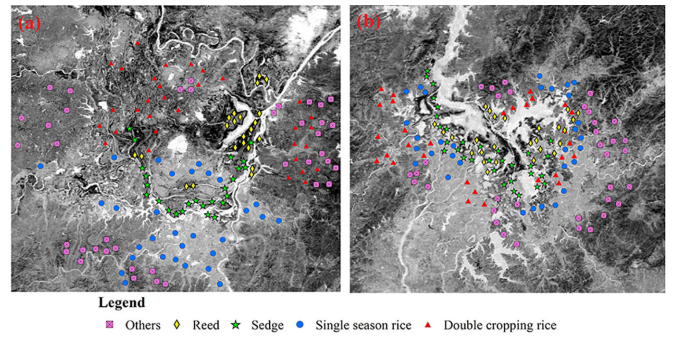


Fig. 2. Distribution of field sites in the Dongting Lake area and the Poyang Lake area.

Fig. 2(a)] in the Dongting Lake area and 30, 29, 26, 29, and 34 in the Poyang Lake area [see Fig. 2(b)], respectively. For some sedge and reed sites, we stood on the road running through the large sedge and reed area, and for other sites, we went to the center of wetland by boat. These field survey samples were used to assess and validate the classification result.

We also selected the 30-m ASTER global digital elevation model (DEM) version 2 and resampled it to a spatial resolution of 250 m. The slope images derived from DEM were used to map paddy rice together with elevation images.

We used the LULC maps (scale: 1:10000) derived from the satellite ZY-3 imagery (3.5 m) together with Google Earth images to collect training and testing samples. The LULC maps were produced by the Bureau of Land and Resources of Hunan Province and Jiangxi Province, China in 2018. The overall accuracy of the LULC product was controlled within 95% by field survey [53].

The rice cropping calendar and rice growth phenological observations are from the Institute of Subtropical Agriculture of China. We also used the paddy rice data of the NLCD 2015, which has a scale of 1:100 000 and divides the land cover into 25 types. NLCD was transformed into a gridded database at 250-m spatial resolution to validate the MODIS-derived paddy rice map.

In this article, we also validated the rice map derived from the MODIS dataset by the data from the Statistical Yearbook of Hunan Province and Jiangxi Province of 2018 (<http://www.hntj.gov.cn/>) at the county level.

III. METHODOLOGY

The proposed paddy rice mapping approach includes six steps (see Fig. 3).

- 1) Smooth the MODIS-EVI time series using the Savitzky-Golay (SG) filter [56].
- 2) Derive several phenological indices from the smoothed EVI time series by the dynamic-threshold method [57].
- 3) Use an improved SVM and the recursive feature elimination (SVM-RFE) method to obtain the optimal image features based on MODIS EVI, phenological variables, LSWI, elevation, and slope images.
- 4) According to the optimized features, discriminate the land cover and crop types by a stacked generalization method.

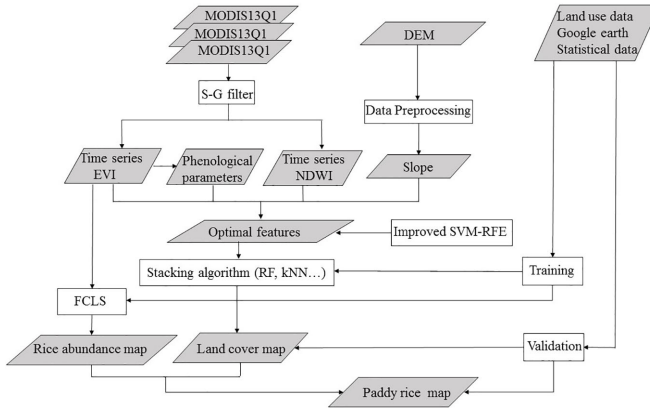


Fig. 3. Flowchart of the proposed rice mapping method.

- 5) Obtain the paddy rice abundance map on the basis of the spectral mixture analysis (the fully constrained least squares, FCLS) using time series MODIS EVI.
- 6) Map the paddy rice using the results of steps 4) and 5).

A. MODIS-EVI Time Series Reconstruction and Phenological Parameter Extraction

The MODIS-EVI data were generated from the synthetic data by the maximum-value composite method, which can reduce the noises caused by cloud and aerosol effects. Note that, the rest noises in the image and inaccurate phenological information were eliminated by an S-G filter using the TIMESAT software [56]. We used the threshold method to derive the phenological variables from the MODIS-EVI time series. The threshold method assumes that a phenological phenomenon occurs if the EVI value is larger than a given threshold [57]. Due to the subtropical monsoon climate, the crops in the study area ripe one or two times per year. Since rice has different growth characteristics with other vegetation, using the fitted EVI time series, we mapped five vegetation phenological parameters, which are the start of the season (SOS), the end of the season (EOS), the length of the season (LOS), the largest EVI value (MOE), and the amplitude of EVI (AOE) during each considered season (see Table II) [56], [57].

B. Feature Optimization

Feature optimization transforms the selected features into a low-dimensional feature space that generates higher accuracy and reduces data redundancy and computational load. The optimal features describing the characteristics of paddy rice were selected from 51 MODIS features (23 EVI images, 23 LSWI images, and 5 phenological parameter images) and 2 DEM features (elevation and slope). The generally used feature extraction methods are filter, wrapper, and embedded models. SVM-RFE is a wrapper approach using the weight magnitude as ranking criterion based on RFE, which has been successfully used to estimate paddy rice phenology and other classification experiments (see Algorithm I) [58].

Algorithm I: SVM-RFE Feature Selection Approach.

Input: (1) Training samples $X = \{x_1, x_2, \dots, x_{n-1}, x_n\}$ (where n is the number of training samples); (2) class label $Y = \{y_1, y_2, \dots, y_{n-1}, y_n\}$.

Output: Feature subset r .

- 1) Initialize: Subset of surviving features $s = [1, 2, \dots, n]$; Feature ranked list $r = []$;
 - Repeat until $s = []$:
 - 2) Restrict training examples to good feature indices $X = X_0(:, s)$;
 - 3) Training $\alpha = \text{SVM-train}(X, Y)$;
 - 4) Compute the weight vector of dimension length(s)
 $w = \sum \alpha_k y_k x_k$
 - 5) Compute the ranking criteria $c_i = (w_i)^2$;
 - 6) Find the feature with smallest ranking criterion $f = \text{argmin}(c)$
 - 7) Update feature ranked list $r = [s(f), r]$;
 - 8) Eliminate the feature with smallest ranking criterion $s = s(1:f-1, f+1:\text{length}(s))$
- End
-

However, using SVM-RFE for feature optimization brings some problems, for example, the correlations between image feature subset described in Algorithm 1 may bring the possible data redundancy [59]. We used an improved feature selection algorithm to address these issues. The improved method consists of three steps: 1) the image features are sorted according to the value of C_i ; 2) generate a feature correlation matrix R with the size of $n \times n$ (n is the number of features); 3) the upper triangular correlation elements r_{ij} are filtered or retained by a given correlation threshold. The final optimal feature subset is then generated

$$R = \begin{bmatrix} r_{11} & r_{12} & \cdots & r_{1n} \\ r_{21} & r_{22} & \cdots & r_{2n} \\ \cdots & \cdots & \ddots & \cdots \\ r_{n1} & r_{n2} & r_{n3} & r_{nn} \end{bmatrix}. \quad (1)$$

C. Rice Mapping by a Stacked Generalization Approach and the Spectral Mixture Method

We first classified the final optimal feature subset by several classifiers, including SVM, random forest (RF), k-nearestneigbor (kNN), extreme gradient boosting (XGB) and DT. According to the natural environment and main vegetation types of the study area, we classified the land cover into eight types: water, sedge, reed, double-cropping rice, single-season rice, rain-fed crop, forest, and others (building, bare land, etc.) [60]. Training samples were selected randomly from Google earth images, the LULC map, and the Sentinel-2 MSI of the region in 2018. Most samples come from Google Earth images and LULC maps. More than 200 samples were selected for each cover type.

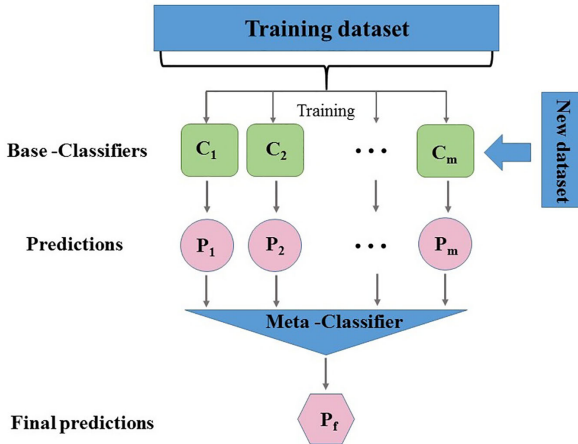


Fig. 4. Concept diagram of Stacking.

We used the stacking algorithm, a generalization method, to improve the accuracy of paddy rice mapping. The stacked generalization fuses the base learning result utilizing “meta-classifier.” In the stacked generalization, there are some individual learners called “base-classifiers,” which are employed to extract the primary feature from the base training dataset and output the secondary training dataset for the secondary learner [52]. In general, the base-classifiers are expected to be diverse and good enough in order to achieve a satisfactory prediction performance. In stacked generalization method, the base-classifiers are first trained using the training dataset. Then, the secondary training dataset is generated by base-classifiers. Finally, the secondary learner (meta-classifier) is trained using the base prediction map that is then employed to produce the final result (Fig. 4). To avoid over-fitting and select the optimal hyper-parameters of different machine learning algorithms, the training samples were divided into k sets of the same size (D_1, D_2, \dots, D_k) by k -fold cross-validation and the stratified sampling method [61]. $K-1$ sets were selected as the training set, and the rest was the test set. The results derived from the test set were then used as the training samples of the secondary classifier. And the classification results of the secondary classifier were taken as the final classification results (see Algorithm II).

The classification accuracy was assessed by a confusion matrix that calculates the overall accuracy, Kappa coefficient as well as the producer and user accuracies. All the field data were employed to validate the classification results.

Pixel mixing is another factor affecting the accuracy of paddy rice information recognition due to the low spatial resolution (250 m) of MODIS images and the complex surface features in study area. In order to accurately extract the paddy rice area in the study sites, a mixture analysis algorithm was used to decompose the mixed MODIS pixels. By this method, the typical EVI curves of different vegetation types were used as the endmember spectra, which were then extracted from highly mixed MODIS data by the constrained particle swarm optimization (PSO) [62]. Endmembers extracted by PSO are purer than that extracted by vertex component analysis (VCA) [62]. The

Algorithm II: Stacking Algorithm.

Input: (1) Training samples $X = \{x_1, x_2, \dots, x_{n-1}, x_n\}$; (2) class label $Y = \{y_1, y_2, \dots, y_{n-1}, y_n\}$; (3) base-learner $\varphi_1, \varphi_2, \dots, \varphi_T$; (4) meta-learner φ .

Output: $H(x) = h'(h_1(x), h_2(x), \dots, h_t(x))$.

- 1) train base-learner h_t :
- for $t = 1, 2, \dots, T$ do
- $h_t = \varphi_t(X, Y)$
- end for
- 2) get each base predict result z_t and meta-learner training set D' :
- for $t = 1, 2, \dots, T$ do
- $z_t = h_t(X)$
- $D' = D' \cup z_t$
- end for
- 3) train the meta-learner $h' = \varphi(D')$.

“mixed endmembers” can be modeled as the combination of the “pure endmembers”

$$S_{VCA} = A_{VCA} * S_{PSO} \quad (2)$$

$$A_{VCA} = f_{unmixing}(S_{VCA}, S_{PSO}) \quad (3)$$

where S_{VCA} is the endmember spectra extracted by VCA, which are regarded as mixed pixels; S_{PSO} is the endmember spectra extracted by PSO, which are regarded as pure pixels; A_{VCA} is the abundance of S_{VCA} , and $f_{unmixing}$ means the unmixing method. The specific process and implement steps can be found in reference [62].

Subsequently, we applied the FCLS [63], [64] to get the unmixing results, and the expression of FCLS is as follows:

$$R_i = \sum_{j=1}^n \rho_j R_{ij} + \varepsilon_i \quad (4)$$

$$\sum_{j=1}^n \rho_j = 1, \rho_j \geq 0 \quad (5)$$

where R_i is the reflectance of i band; ρ_j is the reflectance weight of the j th endmember; R_{ij} is the reflectance of endmember j at i band; ε_i is the residual of i band.

The final paddy rice area in the study area was calculated as

$$A_{rice} = \sum_{i=1}^n (P_i \times F_i) \times 250 \times 250 \times 10^{-4} \quad (6)$$

where A_{rice} is the paddy rice area (hm^2); n , P_i , and F_i are the pixel numbers of rice, corresponding pixel of rice, and abundance value of rice in pixel i . We utilize the NLCD dataset and statistical data to validate the paddy rice area derived from the MODIS time series.

IV. RESULTS AND ANALYSIS

A. Classification Ability of Phenological Parameters Based on Samples

As the smoothed MODIS-EVI time series in Fig. 5 shows, the most stable and longest growing season belongs to forest. The

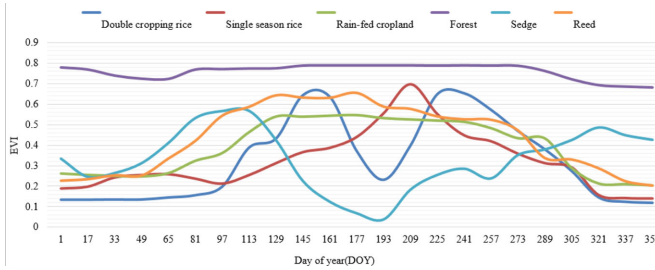


Fig. 5. Smoothed MODIS EVI time series.

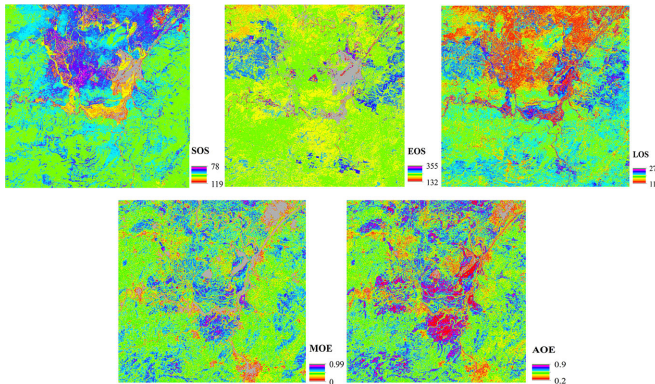


Fig. 6. Phenological parameters of the Dongting Lake area.

rain-fed cropland and reed also have stable and long growing seasons. The EVI value of sedge enjoys a fast growth from day of year (DOY) 1 to DOY113, but drops quickly during DOY113–DOY177. The lowest EVI value of sedge of the year appears on DOY177. The double-cropping rice has the growing peaks on DOY145 and DOY241. The EVI value of the single-season rice climbs fast before DOY209, then plunges. Reed and rain-fed cropland grow relatively quick between DOY1 and DOY129, and the growth becomes slower and stable from DOY129 to DOY257. The EVI value of forest shows no significant change. Since different vegetation types have quite different EVI time series, especially during critical growth stages, they can be identified using the EVI time series.

The phenological variables derived from EVI time series are illustrated in Fig. 6, which plots the values of 50 randomly selected pixel points (based on Google earth images) for six vegetation types in the study area. Forest has a long growing season (~191 days), which starts early (DOY82) and ends late (DOY273). The SOS and EOS of the rain-fed cropland are similar to that of the forest. The single-season rice and double-cropping rice have later SOSs (DOY113 and 98, respectively) and earlier EOSs (DOY256 and 263, respectively) than other vegetation types. Sedge starts growing around March (DOY 75) and finishes growing around October (DOY 274), which is similar to sedge. Forest and the rain-fed cropland have the maximum and minimum EVI, respectively. The EVI values of other vegetation types are very similar. In addition, forest has the minimum seasonal AOE, but rice and sedge have large seasonal AOE.

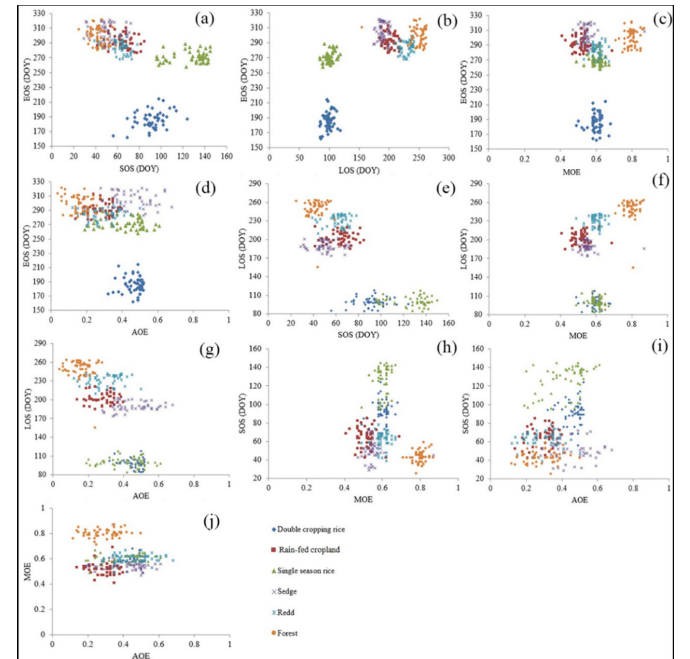


Fig. 7. Classification ability of the phenological parameter combinations.

TABLE I
OPTIMAL CLASSIFICATION FEATURE SUBSETS

Optimal feature subsets	
Improved method	EVI (DOY49, DOY113, DOY193 and DOY241), LSW1 (DOY87 and DOY177), phenological parameters (EOS and SOS), slope
SVM-RFE	EVI (DOY33, DOY49, DOY81, DOY145, DOY113, DOY193, DOY209 and DOY241), LSW1 (DOY87, DOY113, DOY209, DOY225 and DOY177), phenological parameters (EOS, SOS and LOS), slope and DEM.

In order to evaluate the classification ability of the phenological variables, we produced scatter plots by different phenological variable combinations. As Fig. 7(a) and (b) show, the two types of rice are separated from other vegetables, but the rest vegetables are mixed together. So the combinations of EOS-SOS and EOS-LOS can be used for distinguishing paddy rice from other vegetation types. The combinations of EOS-MOE [see Fig. 7(c)] and EOS-AOE [see Fig. 7(d)] can only separate double-cropping rice, and the SOS-MOE [see Fig. 7(h)] and SOS-AOE [see Fig. 7(i)] combinations can only extract single-season rice to a certain degree. Despite the relative clear boundaries among sedge, reed, rain-fed cropland, and forest extracted by the combinations of LOS-MOE [see Fig. 7(f)] and LOS-AOE [see Fig. 7(g)], the two types of rice are mixed. The classification ability of other combinations are relatively weak.

B. Optimal Classification Features

For reducing the data redundancy, an optimal feature combination was generated by the improved feature selection algorithm as shown in Table I. The optimal classification feature subsets are MODIS EVI on DOY49, DOY113, DOY193, and

TABLE II
CLASSIFICATION ACCURACIES AND OPTIMAL PARAMETERS OF SINGLE CLASSIFIER

Algorithms	Optimal parameters	Overall accuracy (%)	Kappa coefficient
RF	n_trees=150	85.3	0.77
kNN	k= 6	87.5	0.83
XGB	n_trees =120, depth=5	85.2	0.78
SVM	C=34, $\gamma=1$	86.0	0.79
DT	---	86.8	0.80

TABLE III
CLASSIFICATION CONFUSION MATRIX OF KNN

	Sedge	Reed	DCR	SSR	Forest	RFC	Others	UA(%)
Sedge	248	2	8	2	5	0	4	92.2
Reed	2	312	6	12	3	2	3	91.2
DCR	0	5	336	22	15	13	0	85.9
SSR	4	6	15	307	3	18	0	87.0
Forest	2	35	0	5	341	12	0	86.3
RFC	0	0	22	16	38	214	0	73.7
Others	3	5	0	0	0	0	393	98.0
PA(%)	96.5	85.5	86.8	84.3	84.2	82.6	98.3	

DCR, SSR, and RFC represent double-cropping rice, single-season rice, and rain-fed cropland.

DOY241, MODIS LSWI on DOY87 and DOY177, phenological parameters of EOS and SOS, as well as the slope data. Compared with the SVM-RFE algorithm, the improved feature selection method can effectively remove the redundancy caused by correlations between the image features.

Apart from the image features shown in Table III, some other features also performed well in vegetation discrimination, such as DEM, phenological parameters of LOS, and some other MODIS EVI. However, these features have a high correlation with the feature subsets selected by the improved method, so they were filtered out.

C. Classification Results and Accuracy Assessment

To get the best classification accuracy of land cover types, we used five classifiers, which are RF, kNN, XGB, SVM, and DT. The classification accuracies shown in Table II demonstrate that all the classifiers have the overall accuracy and Kappa coefficient above 85% and 0.75, respectively. kNN has the highest overall accuracy (87.5%) and Kappa coefficient (0.83). The user accuracy of the kNN algorithm for distinguishing double-cropping rice and single-season rice are 85.9% and 87.0%, respectively (see Table III). There are some misclassification between rice and rain-fed cropland, rice and forest, as well as single-season rice and double-cropping rice. A portion of paddy rice pixels were misclassified as rain-fed cropland, because some crops have the similar phenological characteristics with that of rain-fed cropland. The pixel mixing is another major reason of rice misclassification.

The results of using the above base-classifiers are combined as the input of the secondary layer of the Stacking algorithm. Stacking (RF) denotes the method using the RF algorithm as

TABLE IV
CLASSIFICATION ACCURACIES AND OPTIMAL PARAMETERS OF STACKING ALGORITHM

Algorithms	Optimal parameters	Overall accuracy (%)	Kappa coefficient
RF	n_trees=120	87.7	0.82
kNN	k= 5	89.2	0.84
XGB	n_trees =90, depth=5	90.3	0.86
SVM	C=100, $\gamma=1$	87.2	0.80
DT	---	87.1	0.79

TABLE V
CLASSIFICATION CONFUSION MATRIX OF STACKING (XGB)

	Sedge	Reed	DCR	SSR	Forest	RFC	Others	UA(%)
Sedge	248	2	5	2	2	0	2	95.0
Reed	2	312	2	4	2	0	2	96.3
DCR	0	2	336	11	6	8	0	92.5
SSR	2	2	12	307	2	14	0	90.6
Forest	1	22	0	5	341	8	0	90.0
RFC	0	0	12	10	20	214	0	83.6
Others	0	2	0	0	0	0	393	99.5
PA(%)	98.0	91.2	91.5	90.1	91.6	87.5	98.9	

DCR, SSR, and RFC represent double-cropping rice, single-season rice, and rain-fed cropland.

the meta-classifier. The classification accuracies and optimal parameters of different secondary classifiers in Stacking are shown in Table IV. Stacking (XGB) gets the highest accuracy (90.3%, 0.86). The lowest accuracy is achieved by Stacking (DT) (87.1%, 0.79). The user accuracies of Stacking (XGB) for distinguishing double-cropping rice and single-season rice are 92.5% and 90.0%, respectively, which are 6.6% and 3% higher than that of using the single classifier (kNN) (see Table V). In addition, the overall accuracy and Kappa coefficient of using Stacking model are generally higher than that of using single classifiers. Stacked generalization scheme can be viewed as a more sophisticated version of cross validation and has been shown experimentally to effectively improve the generalization ability of ANN-models over using a single level learning model. In the stacked generalization algorithm, the output result is produced by the meta-classifier based on the predictions of base-classifiers. Therefore, the correlation of different classifiers in base-classifiers may be the main factors impacting the classification accuracy. In general, the changes in classification accuracies caused by different configurations (including different algorithms, different combinations of base-classifiers, and different meta-classifier) of the stacking model are minimal. Thus, to achieve a stable and generalized performance, an adaptive object-based stacked generalization algorithm that can automatically search for the best combination of parameters is needed.

The land cover maps of the Dongting Lake area obtained by different methods are shown in Fig. 8. They are similar except for a few small areas (black ellipse in Fig. 8). The vegetation types in this area are diverse, so vegetation mixed pixels are inevitable. Sedge and reed mainly grow around Dongting Lake, so they are easily separated from the paddy rice. However, there are a

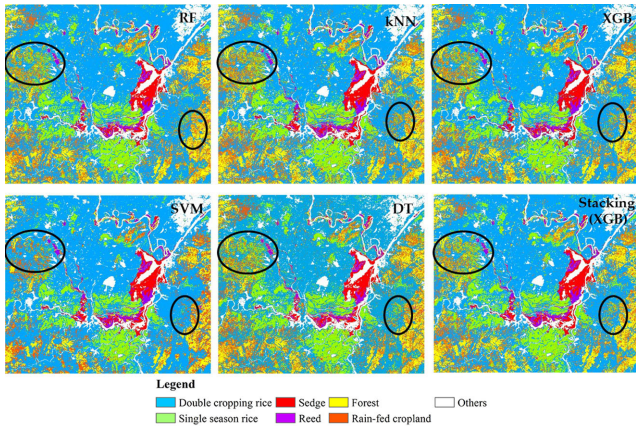


Fig. 8. Land cover maps of the Dongting Lake area.

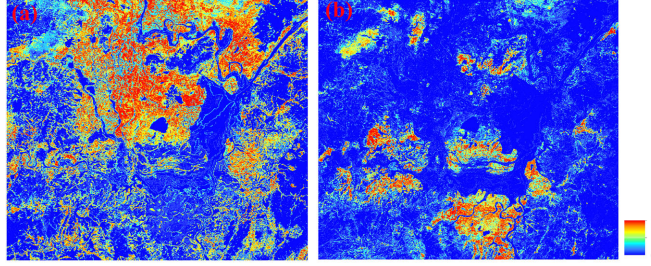


Fig. 9. Abundance map of (a) double-cropping rice and (b) single-season rice.

few mixed pixels in the place where rice grows together with sedge and reed. The pixel mixing is serious between paddy rice and forest and rain-fed cropland, especially crops with similar phenology to rice.

D. Rice Mapping Results and Accuracy Assessments

In this study, the EVI curves of different vegetation types were utilized as the endmember spectra, and FCLS was used to decompose the mixed pixels to obtain the abundance map of rice (see Fig. 9). In the areas with one cropping type (either double-cropping rice or single-season rice), the abundance is relatively large, even close to 1, indicating that the proportion of mixed pixels is small. For the transition region of the two rice types, or the cross-bands, the abundance value is small, that is, the proportion of mixed pixels is large.

The rice distribution map generated by the proposed method is shown in Fig. 10(a). In this region, the double-cropping rice distributes much wider than the single-season rice, especially in the north part with dense river networks and lakes. However, the single-season rice mainly grows around Dongting Lake or along rivers, and it has sporadic distribution across the study area.

From Figs 9 and 10(a), we finally derived the area of the paddy rice in the Dongting lake area. The correlation analysis shows that the MODIS-derived rice area has a strong correlation (the determination coefficient 0.9975) with that of the government statistics at the county level for the year of 2018. The determination coefficient (R^2) of the regression model in

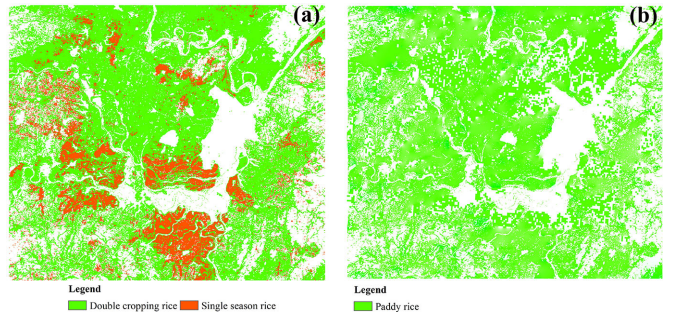


Fig. 10. Paddy rice derived from (a) the MODIS time series and (b) the NLCD product.

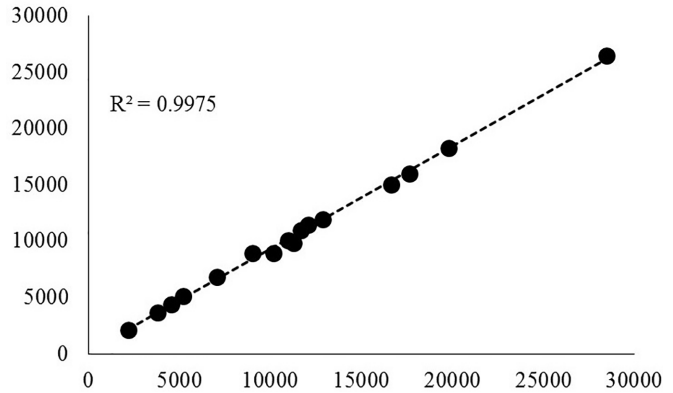


Fig. 11. Regression analysis between the MODIS-derived rice area and statistics data.

TABLE VI
RE BETWEEN THE MOD AND THE GRA STATISTICS

County/District	MOD(ha)	GRA(ha)	REA(%)
Huarong	16650	15015	10.9
Pingjiang	11689	11002	6.2
Junshan	2198	2119	3.7
Anxiang	5201	5098	2.0
Hanshou	17630	16026	10.0
Shimen	4568	4405	3.7
Linli	9036	8969	0.7
Nanxiang	12064	11428	5.6
Anhua	3825	3652	4.7
Taojiang	10145	8908	13.9
Dingcheng	12882	11908	8.2
Ningxiang	19769	18295	8.1
Wuling	10988	10108	8.7
Miluo	28485	26486	7.5
Xiangyin	11248	9826	14.5
Jingshi	7058	6815	3.6

Fig. 11 indicates that the model could explain the variability in the data. In general, the paddy rice area derived from MODIS data has slight overestimations, and the average relative error (RE) is about 7%. The RE between the MODIS-derived rice areas (MOD) and the government's rice area (GRA) statistics ranges from 2.0% to 14.5% (see Table VI), which may be caused

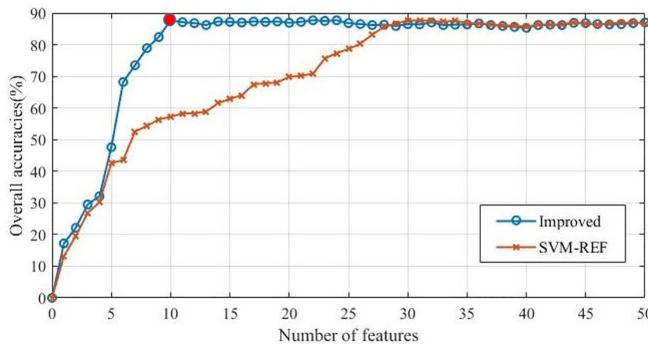


Fig. 12. Classification accuracy of kNN using the features obtained by different feature selection methods.

by the overestimation of MOD. Counties/districts with larger rice distribution area have larger RE between the classification results and statistical data. For example, the RE of counties with a rice distribution area of more than 10 000 ha is generally larger than 7.5%. However, this does not mean that the larger the rice distribution area, the greater the RE. The rice distribution area of Xiangyin County is 11 248 ha, which is 17 237 ha smaller than that of Miluo County. However, the paddy rice estimation RE of Xiangyin County is twice of that of Miluo County. Part of the reason for this phenomenon is that the MODIS-derived rice areas was calculated by pixel counts, while the GRA statistics was estimated by the total sown area.

V. DISCUSSION

A. Comparison Between the Improved Feature Selection Method and SVM-RFE

In order to estimate the efficacy of the improved feature selection method, we compared it with SVM-RFE in terms of the classification accuracy of their selected features. These two feature selection methods are independent of the classifier, only kNN classifier was reported. Since the results of other classifiers are similar to kNN, their results are not provided. As shown in Fig. 12, based on the highest accuracies achieved by the SVM-RFE and the improved method, the dimensions of the optimal features are 9 and 18, respectively. The results demonstrate that the improved feature selection method can filter some related features, which will reduce the data redundancy. Moreover, the improved feature selection method can determine the optimal features by the red dot shown in Fig. 12, whereas other methods (such as mRMR, FSDD, and CFS4) have to compare the classification accuracy of different numbers of features to get the optimal features, which involves a lot of computation [59]. This means the improved feature selection method has higher efficiency than other methods.

B. Stability and Generalization of the Stacking Algorithm

We utilized another commodity grain base (Poyang Lake area) of China to evaluate the stability of the stacking algorithm. The Poyang Lake area also has the subtropical monsoon climate, with complex and diverse vegetation types, which is very suitable

TABLE VII
CLASSIFICATION ACCURACIES AND OPTIMAL PARAMETERS OF SINGLE CLASSIFIERS

Algorithms	Optimal parameters	Overall accuracy (%)	Kappa coefficient
RF	n_trees=150	84.9	0.76
kNN	k= 5	87.2	0.83
XGB	n_trees =120, depth=5	85.8	0.77
SVM	C=50, $\gamma=1$	86.5	0.80
DT	---	84.7	0.80

TABLE VIII
CLASSIFICATION ACCURACIES AND OPTIMAL PARAMETERS OF STACKING ALGORITHMS

Algorithms	Optimal parameters	Overall accuracy (%)	Kappa coefficient
RF	n_trees=120	86.9	0.81
kNN	k= 5	87.8	0.84
XGB	n_trees =100, depth=5	88.5	0.86
SVM	C=100, $\gamma=1$	88.1	0.80
DT	---	86.3	0.79

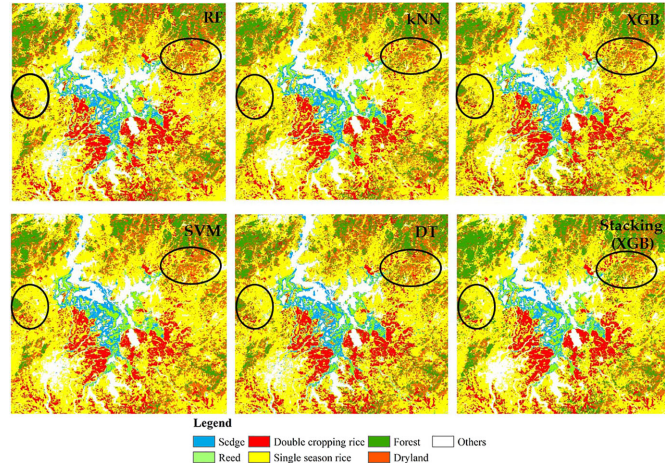


Fig. 13. Land cover maps of Poyang Lake area.

for testing the stability of the stacking model. The classification accuracies and optimal parameters of single classifiers and stacking combination models are presented in Tables VII and VIII, respectively. The kNN classifier has higher overall accuracy (87.2%) and Kappa coefficient (0.83) than other single classifiers, which is the same to the results of the Dongting Lake area. The highest overall accuracy is also obtained by Stacking (XGB). Therefore, the Stacking algorithm has good robustness and stability.

As shown in Fig. 13, the land cover maps obtained by different classifiers are very similar except for some small areas. Overall, the stacking (XGB) has a better performance than single classifiers due to the strong generalization ability of the stacking model.

As Table VII shows, DT gets the lowest overall accuracy (84.7%), so we only used the results obtained by RF, kNN, XGB, and SVM as the training dataset to do the land cover classification (see Table IX). The best results is obtained by

TABLE IX
CLASSIFICATION ACCURACIES AND OPTIMAL PARAMETERS OF
STACKING ALGORITHM

Algorithms	Optimal parameters	Overall accuracy (%)	Kappa coefficient
RF	n_trees=120	87.2	0.81
kNN	k= 5	86.9	0.84
XGB	n_trees =100, depth=5	88.2	0.86
SVM	C=100, $\gamma=1$	88.1	0.80

staking (XGB), with the overall accuracy of 88.2%, lower than that in Table VIII. But the accuracy of the stacking (RF) has been improved slightly (0.3%). Generally, the classification results considering DT is better than that doesn't consider DT. By combining the results of different classifiers, the generalization ability of the stacking model is improved, which is also one of the advantages of the ensemble learning.

C. Merits and Demerits of the Proposed Method

As an important food and wetland plant on the earth, paddy rice plays a significant role in food security and regional ecology. In this study, we used a stacked generalization approach and spectral mixture method to generate paddy rice maps from coarse resolution images. The method employs time series MODIS in the growing stages of paddy rice, water index, and elevation images, as well as the phenology variables derived from MODIS time series. This approach considers the soil and canopy characteristics of paddy rice during the critical growth phases of rice and also the generalization ability of stacking algorithm. The results show that the proposed method could achieve high accuracies in paddy rice mapping at large scales. Compared with the studies using MODIS dataset and the pixel-based method in the study regions with similar conditions, our approach can achieve similar or higher classification accuracies [4], [17], [18], [27], [36], [38], [45]. The determination coefficient (R^2) between the MODIS-derived rice and statistical data have also been increased by the proposed method [17], [18], [38].

A number of factors could affect the accuracy of paddy rice mapping when using the proposed method. One is the temporal resolution of the MOD13Q1 dataset. The 16-day MODIS time series EVI was generated by the maximum value of each individual pixel in a period of 16 days [17]. In this process, some information in the paddy rice growth stage may loss. Using daily MODIS data can improve the growth phase identification, but would result in larger datasets and cloud contamination. Another factor is the residual cloud contamination in the 16-day MODIS time series EVI, which is quite common in tropical and subtropical areas. Synthetic aperture radar (SAR) is a promising way in mapping paddy rice, because of its well-timed image acquisitions and independence of meteorological conditions. However, it is expensive to acquire time-series SAR images covering large-scale areas. The third factor is the selection of machine learning classifiers in the stacking algorithm. In this study, we chose five frequently-used machine learning classifiers, and more machine learning classifiers will be used in future researches.

VI. CONCLUSION

In this study, a stacked generalization approach and the spectral mixture method were employed to map paddy rice using time series MODIS EVI data of the Dongting Lake area. The result has demonstrated that the proposed method can map large scale paddy rice using coarse spatial resolution images. Despite the influence of cloud cover, mixed pixels and other potential issues, the overall accuracy and Kappa efficient are higher than 90.3% and 0.86, respectively. The results are reaffirmed by the strong correlation between the derived rice area and the government rice area statistics at the county level ($R^2 > 0.9$). The rice area derived from the MODIS data is slightly overestimated, with an RE between 2.0% and 14.5%. Our paddy rice mapping algorithm focuses on the detection of growth stages of the paddy rice, and it provides spatial distribution with acceptable accuracy of paddy rice in other large-scale areas.

ACKNOWLEDGMENT

The authors would like to thank the editors and anonymous reviewers for the valuable comments, which are significant for improving this article.

REFERENCES

- [1] E. Elert, "Rice by the numbers: A good grain," *Nature*, vol. 514, pp. 50–51, 2014.
- [2] M. X. Liu, X. N. Liu, L. Wu, X. Zou, T. Jiang, and B. Zhao, "A modified spatiotemporal fusion algorithm using phenological information for predicting reflectance of paddy rice in southern China," *Remote Sens.*, vol. 10, no. 772, pp. 1–22, 2018.
- [3] J. Dong and X. Xiao, "Evolution of regional to global paddy rice mapping methods: A review," *ISPRS J. Photogramm. Remote Sens.*, vol. 119, pp. 214–227, 2016.
- [4] N. T. Son, C. F. Chen, C. R. Chen, H. N. Duc, and L. Y. Chang, "A phenology-based classification of time-series MODIS data for rice crop monitoring in mekong delta, Vietnam," *Remote Sens.*, vol. 6, no. 1, pp. 135–156, 2013.
- [5] J. R. Beddington *et al.*, "Achieving food security in the face of climate change: Summary for policy makers from the commission on sustainable agriculture and climate change," *Cgiar Res. Program Climate Change Agriculture Food Secur.*, 2011.
- [6] B. Bouman and T.P. Tuong, "Field water management to save water and increase its productivity in irrigated lowland rice," *Agricultural Water Manage.*, vol. 49, pp. 11–30, 2001.
- [7] D. H. Mao *et al.*, "China's wetlands loss to urban expansion," *Land Degradation Develop.*, vol. 29, pp. 2644–2657, 2018.
- [8] D. H. Mao *et al.*, "Conversions between natural wetlands and farmland in China: A multiscale geospatial analysis," *Sci. Total Environ.*, vol. 634, pp. 550–560, 2018.
- [9] Y. Zhou *et al.*, "Mapping paddy rice planting area in rice-wetland coexistent areas through analysis of Landsat 8 OLI and MODIS images," *Int. J. Appl. Earth Observ. Geoinf.*, vol. 46, pp. 1–12, 2016.
- [10] M. K. Mosleh and Q. K. Hassan, "Development of a remote sensing-based "boro" Rice mapping system," *Remote Sens.*, vol. 6, pp. 1938–1953, 2014.
- [11] M. A. Friedl *et al.*, "Global land cover mapping from MODIS: Algorithms and early results," *Remote Sens. Environ.*, vol. 83, pp. 287–302.
- [12] S. Bontemps, P. Defourny, V. B. Eric, O. Arino, V. Kalogirou, and J. R. Perez, "GLOBCOVER: Products description and validation report," *Foro Mundial. De. La. Salud.*, vol. 17, pp. 285–287, 2008.
- [13] W. Li, P. Ciais, N. Macbean, S. S. Peng, P. Defourny, and S. Bontemps, "Major forest changes and land cover transitions based on plant functional types derived from the ESA CCI Land Cover product," *Int. J. Appl. Earth Observ. Geoinf.*, vol. 47, pp. 30–39, 2016.
- [14] F. Gerald, C. Christopher, T. Michael, T. UIImann, and E. Zoungrana, "Integration of optical and synthetic aperture radar imagery for improving crop mapping in northwestern Benin, West Africa," *Remote Sens.*, vol. 6, no. 7, pp. 6472–6499, 2014.

- [15] D. Bachelet, "Rice paddy inventory in a few provinces of China using AVHRR data1," *Geocarto Int.*, vol. 10, pp. 23–38, 1995.
- [16] M. Boschetti, D. Stroppiana, P. A. Brivio, and S. Bocchi, "Multi-year monitoring of rice crop phenology through time series analysis of MODIS images," *Int. J. Remote Sens.*, vol. 30, pp. 4643–4662, 2009.
- [17] X. Xiao *et al.*, "Mapping paddy rice agriculture in southern China using multi-temporal MODIS images," *Remote Sens. Environ.*, vol. 95, pp. 480–492, 2005.
- [18] X. Xiao *et al.*, "Mapping paddy rice agriculture in South and Southeast Asia using multi-temporal MODIS images," *Remote Sens. Environ.*, vol. 100, pp. 95–113, 2006.
- [19] C. F. Chen, N. T. Son, L. Y. Chang, and C. R. Chen, "Classification of rice cropping systems by empirical mode decomposition and linear mixture model for time-series MODIS 250 m NDVI data in the Mekong Delta, Vietnam," *Int. J. Remote Sens.*, vol. 32, pp. 5115–5134, 2011.
- [20] K. Pittman, M. C. Hansen, I. Becker-Reshef, P. V. Potapov, and C. O. Justice, "Estimating global cropland extent with multi-year MODIS data," *Remote Sens.*, vol. 2, pp. 1844–1863, 2010.
- [21] D. Peng, A. R. Huete, J. Huang, F. Wang, and H. Sun, "Detection and estimation of mixed paddy rice cropping patterns with MODIS data," *Int. J. Appl. Earth Observ. Inf.*, vol. 13, pp. 13–23, 2011.
- [22] P. S. Thenkabail, "Mapping rice areas of South Asia using MODIS multitemporal data," *J. Appl. Remote Sens.*, vol. 5, pp. 863–871, 2011.
- [23] X. J. Xu *et al.*, "Evaluation of one-class support vector classification for mapping the paddy rice planting area in Jiangsu province of China from landsat 8 OLI imagery," *Remote Sens.*, vol. 10, no. 4, pp. 546–568, 2018.
- [24] Y. Li, "Study on methods of rice planting area estimation at regional scale using NOAA/AVHRR data," *J. Remote Sens.*, vol. 2, no. 2, pp. 125–130, 1998.
- [25] R. Sianturi, V. G. Jetten, J. Ettema, and J. Sartohadi, "Distinguishing between hazardous flooding and non-hazardous agronomic inundation in irrigated rice fields: A case study from west java," *Remote Sens.*, vol. 10, no. 1003, pp. 1–24, 2018.
- [26] N. T. Son, C. F. Chen, C. R. Chen, V. Q. Minh, and N. H. Trung, "A comparative analysis of multitemporal MODIS EVI and NDVI data for large-scale rice yield estimation," *Agricultural Forest Meteorol.*, vol. 197, pp. 52–64, 2014.
- [27] T. Sakamoto, P. V. Cao, N. V. Nguyen, A. Kotera, and M. Yokozawa, "Agro-ecological interpretation of rice cropping systems in flood-prone areas using MODIS imagery," *Photogram. Eng. Remote Sens.*, vol. 75, pp. 413–424, 2009.
- [28] T. Sakamoto, M. Yokozawa, H. Toritani, M. Shibayama, N. Ishitsuka, and H. Ohno, "A crop phenology detection method using time-series MODIS data," *Remote Sens. Environ.*, vol. 96, pp. 366–374, 2005.
- [29] B.D. Wardlow and S.L. Egbert, "Large-area crop mapping using time-series MODIS 250m NDVI data: An assessment for the U.S. Central Great Plains," *Remote Sens. Environ.*, vol. 112, pp. 1096–1116, 2008.
- [30] G. L. Galford, J. F. Mustard, J. Melillo, A. Gendrin, C. C. Cerri, and C. E. Cerri, "Wavelet analysis of MODIS time series to detect expansion and intensification of row-crop agriculture in Brazil," *Remote Sens. Environ.*, vol. 112, pp. 576–587, 2008.
- [31] K. Pittman, M. C. Hansen, I. Beckerreshef, P.V. Potapov, and C.O. Justice, "Estimating global cropland extent with multi-year MODIS data," *Remote Sen.*, vol. 2, pp. 1844–1863, 2010.
- [32] D. Vittorio, A. Courtney, and A. P. Georgakakos, "Land cover classification and wetland inundation mapping using MODIS," *Remote Sens. Environ.*, vol. 204, pp. 1–17, 2018.
- [33] J. A. Foley, "Global consequences of land use," *Science*, vol. 309, pp. 570–574, 2005.
- [34] M. Z. Alhamdan *et al.*, "Evaluating land cover changes in Eastern and Southern Africa from 2000 to 2010 using validated Landsat and MODIS data," *Int. J. Appl. Earth Observ. Inf.*, vol. 62, pp. 8–26, 2017.
- [35] S. Asilo, K. D. Bie, A. Skidmore, A. Nelson, M. Barbieri, and A. Maunhan, "Complementarity of two rice mapping approaches: Characterizing strata mapped by hypertemporal MODIS and rice paddy identification using multitemporal SAR," *Remote Sens.*, vol. 6, pp. 12789–12814, 2014.
- [36] P.S. Thenkabail, "Mapping rice areas of South Asia using MODIS multitemporal data," *J. Appl. Remote Sens.*, vol. 5, pp. 863–871, 2011.
- [37] H. Wang, J. Chen, Z. Wu, and H. Lin, "Rice heading date retrieval based on multitemporal MODIS data and polynomial fitting," *Int. J. Remote Sens.*, vol. 33, pp. 1905–1916, 2012.
- [38] P. Teluguntla, D. Ryu, B. George, J. Walker, and H. Malano, "Mapping flooded rice paddies using time series of MODIS imagery in the Krishna river basin, India," *Remote Sens.*, vol. 7, pp. 8858–8882, 2015.
- [39] K. Chumkesornkulkit, T. Kasetkasem, P. Rakwatin, A. Eiumnoh, and I. Kumazawa, "Estimated rice cultivation date using an extended Kalman filter on MODIS NDVI time-series data," in *Proc. IEEE Int. Conf. Elect. Eng./Electron., Comput., Telecommun. Inf. Technol.*, 2013, pp. 1–6.
- [40] V. Tomar, "Rice equivalent crop yield assessment using MODIS sensors' based MOD13A1-NDVI data," *IEEE Sensors J.*, vol. 14, no. 10, pp. 3599–3605, Oct. 2014.
- [41] M. K. Gumma, A. Nelson, P. S. Thenkabail, and A. S. Singh, "Mapping rice areas of south Asia using MODIS multitemporal data," *J. Appl. Remote Sens.*, vol. 5, pp. 863–871, 2011.
- [42] T. Motohka, K. N. Nasahara, A. Miyata, M. Mano, and S. Tsuchida, "Evaluation of optical satellite remote sensing for rice paddy phenology in monsoon Asia using a continuous in situ dataset," *Int. J. Remote Sens.*, vol. 30, pp. 4343–4357, 2009.
- [43] A. O. Onojeghuo, G. A. Blackburn, Q. M. Wang, P. M. Atkinson, D. R. Kindred, and Y. X. Miao, "Rice crop phenology mapping at high spatial and temporal resolution using downsampled MODIS time-series," *Glaci. Remote Sens.*, vol. 14, pp. 1548–1603, 2018.
- [44] T. Sakamoto, N. V. Nguyen, H. Ohno, and N. Ishitsuka, and M. Yokozawa "Spatio-temporal distribution of rice phenology and cropping systems in the Mekong Delta with special reference to the seasonal water flow of the Mekong and Bassac rivers," *Remote Sens. Environ.*, vol. 100, pp. 1–16, 2006.
- [45] T. Sakamoto, C. Van Phung, A. Kotera, K. D. Nguyen, and M. Yokozawa, "Analysis of rapid expansion of inland aquaculture and triple rice-cropping areas in a coastal area of the Vietnamese Mekong delta using MODIS time-series imagery," *Landscape Urban Plan.*, vol. 92, pp. 34–46, 2009.
- [46] M. K. Mosleh, Q. K. Hassan, and E. H. Chowdhury, "Application of remote sensors in mapping rice area and forecasting its production: A review," *Sensors (Basel)*, vol. 15, pp. 769–791, 2015.
- [47] X. Wang *et al.*, "Land-cover classification of coastal wetlands using the RF algorithm for worldview-2 and landsat 8 images," *Remote Sens.*, vol. 11, 2019, Art. no. 1927.
- [48] J. H. Friedman, "Greedy function approximation: A gradient boosting machine," *Ann. Statist.*, vol. 29, pp. 1189–1232, 2001.
- [49] S. Q. Yang and L.H. Zhao, "Application of stochastic forest algorithm in urban air quality prediction," *Statist. Decis.*, vol. 20, pp. 83–86, 2017.
- [50] H. Hui, W. J. Wang, and H. S. Guo, "A SVM bagging integrated method based on feature selection," *Microcomput. Syst.*, vol. 35, pp. 2533–2537, 2014.
- [51] X. H. Zhao, J. B. Xia, and M. H. Li, "Network traffic classification based on stochastic forest," *Proc. CSEE*, vol. 8, pp. 184–190, 2013.
- [52] D. H. Wolpert, "Stacked generalization," *Neural Networks*, vol. 5, pp. 241–259, 1996.
- [53] M. Zhang, H. Lin, G. Wang, H. Sun, and J. Fu, "Mapping paddy rice using a convolutional neural network (CNN) with landsat 8 datasets in the Dongting lake area, China," *Remote Sens.*, vol. 10, 2018, Art. no. 1840.
- [54] C. A. Petri and L. S. Galvão, "Sensitivity of seven MODIS vegetation indices to BRDF effects during the Amazonian dry season," *Remote Sens.*, vol. 11, 2019, Art. no. 1650.
- [55] F. Marzialetti S. Giulio, M. Malavasi, M. G. Sperandii, A. T. R. Acosta, and M. L. Carranza, "Capturing coastal dune natural vegetation types using a phenology-based mapping approach: The potential of sentinel-2," *Remote Sens.*, vol. 11, 2019, Art. no. 1506.
- [56] P. Jönsson and L. Eklundh, "A program for analyzing time-series of satellite sensor data," *Comput. Geosci.*, vol. 30, pp. 833–845, 2004.
- [57] J. Kang, X. H. Hou, Z. Niu, S. Gao, and K. Jia, "Decision tree classification based on fitted phenology parameters from remotely sensed vegetation data," *Trans. Chin. Soc. Agricultural Eng.*, vol. 30, pp. 148–156, 2014.
- [58] K. Çağlar, T. Gülsen, and E. Erten, "Paddy-rice phenology classification based on machine-learning methods using multitemporal co-polar X-Band SAR images," *IEEE J. Sel. Topics Appl. Earth Observ. Remote Sens.*, vol. 9, no. 6, pp. 2509–2519, Jun. 2016.
- [59] Y. Zhi, S. Yun, K. Li, Q. B. Liu, L. Liu, and B. Brian, "An improved scheme for rice phenology estimation based on time-series multispectral HJ-1A/B and polarimetric RADARSAT-2 data," *Remote Sens. Environ.*, vol. 195, pp. 184–201, 2017.
- [60] M. Zhang, N. Zeng, and Y.S. Zhu, "Wetland mapping of Dongting Lake Basin based on time-series MODIS data and object-based method," *J. Remote Sens.*, vol. 13, pp. 178–185, 2015.
- [61] R. Filgueiras, E.C. Mantovani, D. Althoff, E.I. Fernandes Filho, and F. F. Cunha, "Crop NDVI monitoring based on sentinel 1," *Remote Sens.*, vol. 11, 2019, Art. no. 1441.

- [62] M. Xu, B. Du, and Y.G. Fan, "Endmember extraction from highly mixed data using linear mixture model constrained particle swarm optimization," *IEEE Trans. Geosci. Remote Sens.*, vol. 57, no. 8, pp. 5502–5511, Aug. 2019.
- [63] U. Kumar *et al.*, "Exploring subpixel learning algorithms for estimating global land cover fractions from satellite data using high performance computing," *Remote Sens.*, vol. 9, no. 1105, pp. 1–24, 2017.
- [64] Y. Cai, M. Zhang, and H. Lin, "Estimation the urban fractional vegetation cover using an object-based mixture analysis method and Sentinel-2 MSI imagery," *IEEE J. Sel. Topics Appl. Earth Observ. Remote Sens.*, vol. 13, pp. 341–350, Jan. 2020.



Meng Zhang received the M.S. degree in geography from Hunan Normal University, Changsha, China, in 2014, and the Ph.D. degree in cartography and geographic Information engineering from Central South University, Changsha, in 2018.

He is currently a Teacher with the College of Forestry, Central South University of Forestry and Technology, Changsha. He has authored more than 15 research papers index by SCI and EI. His research interests include resources and environment remote sensing and GIS.



Huaiqing Zhang received the M.S. and Ph.D. degrees in forest management from the Chinese Academy of Forestry (CAF), Beijing, China, in 1998 and 2001, respectively.

He is currently a Professor, Chief Expert on visualization and simulation, and Director with the Department of Visualization Simulation and Monitoring, Institute of Forest Resource Information Techniques, Chinese Academy of Forestry, Beijing, China. His major research interests include forest visualization and simulation techniques, and monitoring of wetland resource using satellite and ground based sensors.



Xinyu Li received the B.S. and M.S. degrees in forestry in 2007 from the Central South University of Forestry and Technology (CSUFT), Changsha, China, where he is currently working toward the Ph.D. degree in forestry remote sensing.

His research interests include image classification and biomass estimation.



Yang Liu received the B.S. degree in digital media technology from Harbin Normal University, Harbin, China, in 2017. She is currently working toward the master's degree at Institute of Forest Resource Information Techniques, Chinese Academy of Forestry, Beijing, China.

Her major research interests include satellite and ground based sensors for wetland resource monitoring.



Yaotong Cai received the B.S. degree in forestry in 2018 from the Central South University of Forestry and Technology (CSUFT), Changsha, China, where he is currently working toward the master's degree in forestry remote sensing.

His research interests include image classification and biomass estimation.



Hui Lin received the B.S., M.S., and Ph.D. degrees in forest management from Central South University of Forestry and Technology, Changsha, China, in 1988, 1991, and 2005, respectively.

She is a Professor with the College of Forestry, CSUFT. She has authored more than 170 research papers published in which 30 papers indexed by SCI. Her research interests include forest remote sensing and GIS.